Figure S1. Related to Figure 1

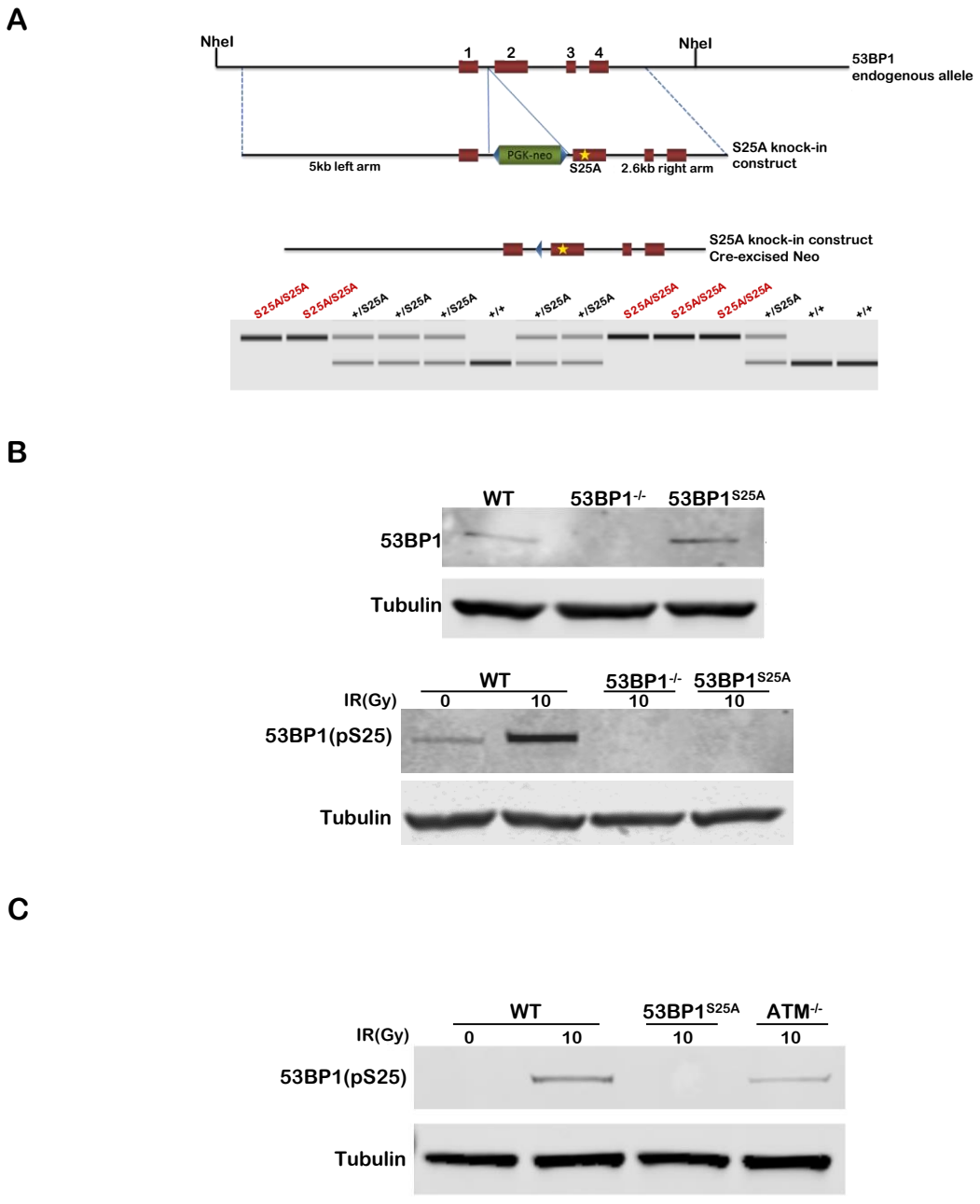

Fig. S1.

53BP1^{S25A} targeting construct and mutant protein expression

(A) Top: Schematic representation of knock-in construct before and after Cre-excision of PGK-neo cassette. Bottom: Representative gel showing PCR genotyping of pups derived from *53BP1$^{S25A/+}$* intercrosses. (B) Top: Western blot analysis of 53BP1 protein expression in B cells derived from WT, *53BP1$^{-/-}$* and *53BP1^{S25A}* mice. Bottom: Western blot analysis of 53BP1 phosphorylation on the Serine 25 residue (pS25) using a phospho-specific antibody. B cells from the indicated genotypes were irradiated with 10 Gy and harvested 1 hour later. Tubulin expression is shown below as the loading control. (C) Western blot analysis of 53BP1 phosphorylation on Serine 25 (pS25) and its dependency on ATM. B cells from the indicated genotypes were irradiated with 10 Gy and harvested 1 hour later. Tubulin expression is shown below as the loading control.

Figure S2. Related to Figure 2

A

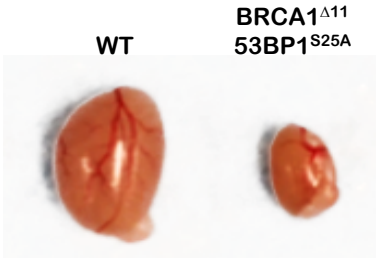

B

MOUSE	AGE DEATH	PHENOTYPE AT DEATH TIME
9849	1y 2mo	Trombus in heart, inflammation in liver, lymphoid hyperplasia, spinal cord vaculation, gray and rough hair coat
9929	5mo	Blindness, degeneration of seminiferous tubules
9947	6mo 3wk	Cloudy eyes, hunched posture, slow mobility, granulocytic hyperplasia
10459	1y 10mo	Left eye blind, white spot/hair in belly, rough hair coat, distended abdomen and lump on left side, hepatocellular carcinoma
11807	3wk	Found dead. No data
10908	7mo	Cloudy eyes, rough hair coat and white spots, lymphocyte infiltrates, mild LN hyperplasia
11933	4mo	Decreased activity, hunched posture, thin, prolapsed penis
10086	1y 10mo	Distended abdomen, rough hair coat, histiocytic sarcoma, atypical hepatocytes and epithelial cells lining tubules
11588	3wk	Found dead. No data
12090	7mo	Decreased activity, hunched posture, thin, rough hair coat, distended abdomen
13393	3mo 2wk	Blind, eye infection, thin, LN and spleen hyperplasia
11141	1y 7mo	White hair spots, rough hair coat, hunched posture, kinked on tail. Open wound on back. Subcutaneous sarcoma, mild karyomegaly in kidneys and liver

C

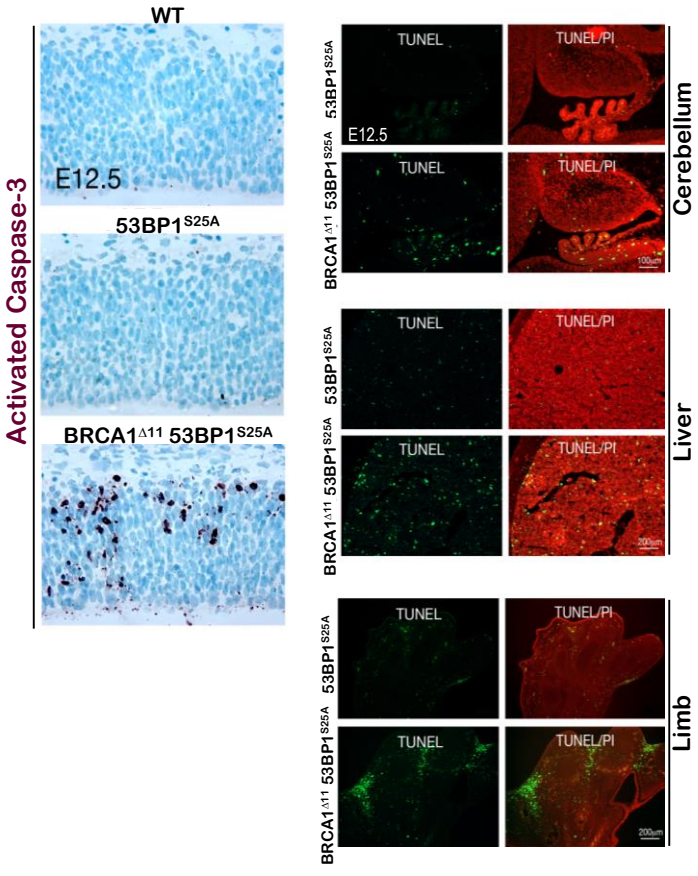

D

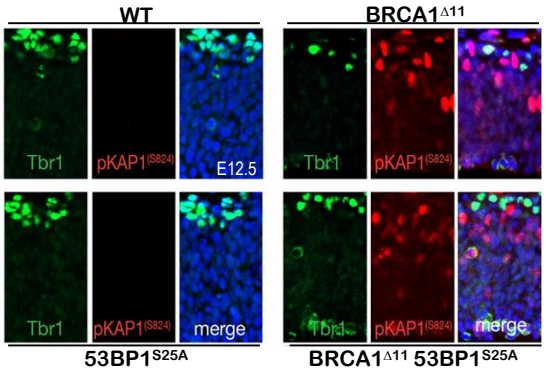

E

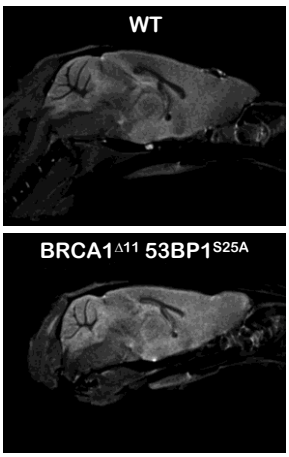

Fig. S2.

Reduced testes size, accelerated aging, increased apoptosis and DNA damage signaling in *BRCA1$^{\Delta 11}$53BP1^{S25A}* mice. (A) Image showing reduced testes size in *BRCA1$^{\Delta 11}$53BP1^{S25A}* mouse compared with WT littermate. (B) Table summarizing the age and phenotypes presented by *BRCA1$^{\Delta 11}$53BP1^{S25A}* mice at the time of death. (C) Immunohistochemical (IHC) identification of apoptosis via activated Caspase-3 or TUNEL staining. Disruption of *BRCA1* causes widespread apoptosis in the developing E12.5 cortical region. The cerebellar region also shows increased cell death in the *BRCA1* mutants. Apoptosis also occurs outside of the nervous system, with elevated levels in the liver and limb bud. Caspase-3 IHC images are colorimetric VIP-staining and methyl green counter-staining, while the TUNEL images are fluorescent with propidium iodide (PI) counter staining. (D) Ongoing DNA damage signaling is present in *BRCA1* mutant cells as indicated by pKAP1(S824) immunostaining. Co-staining with Tbr1 indicates much of the DNA damage is occurring in the developing neurons of the E12.5 neocortex. Merged images are counterstained using DAPI. (E) MRI analysis reveals a reduction in volume of the 2 months-old mutant brain compared to the control.

Figure S3. Related to Figure 3

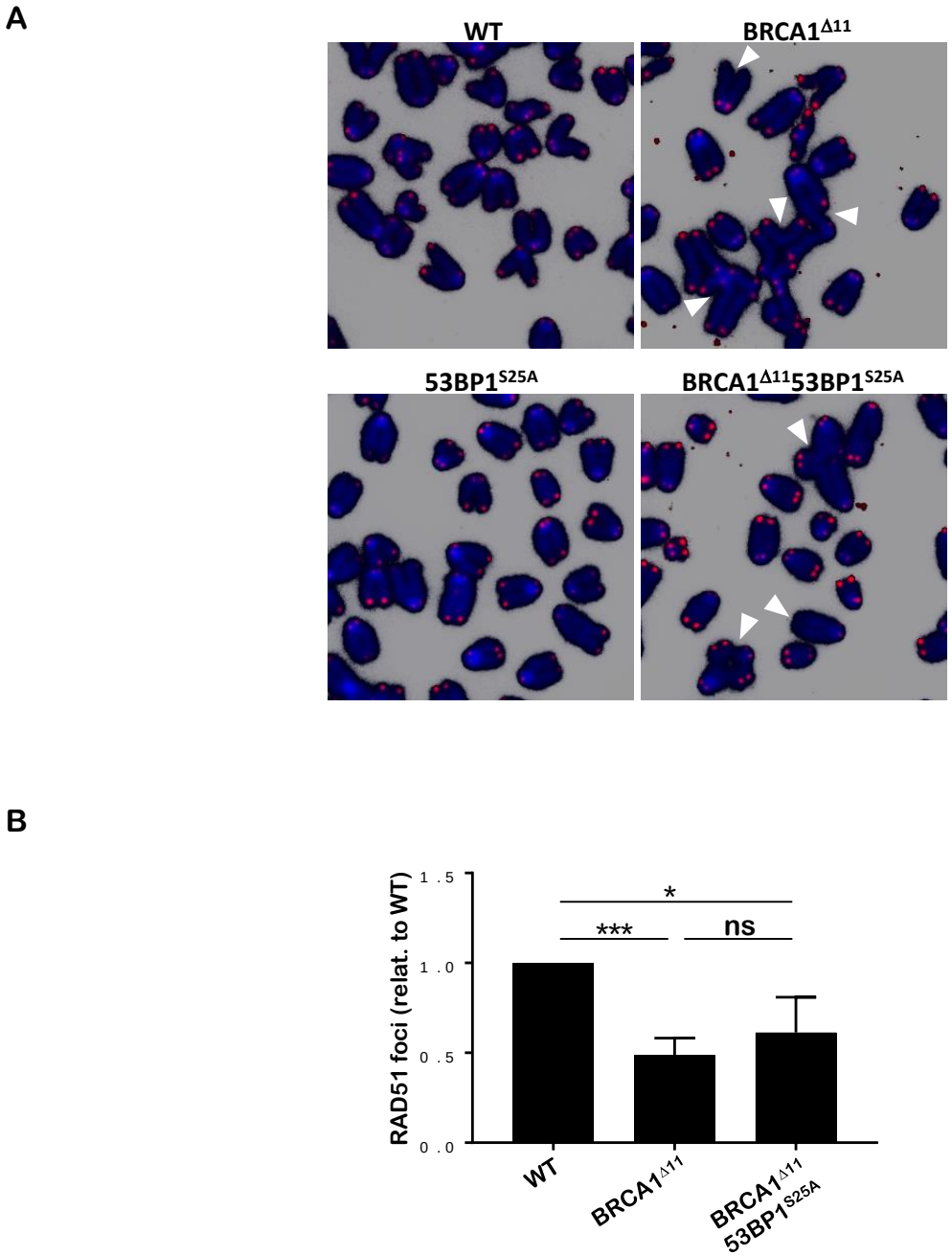

Fig. S3.
***BRCA1$^{\Delta 11}$53BP1^{S25A}* cells accumulate chromosomal aberrations in response to PARPi and show impaired RAD51 recruitment**

(A) Representative images of metaphase spreads from MEFs of the indicated genotypes. Cells were treated with 1 μM PARPi overnight and chromosomal aberrations were detected by FISH. Blue is DAPI-stained DNA and red marks telomeric DNA. Arrow heads indicate chromosomal aberrations characteristic of cells lacking functional BRCA1. (B) Quantification of RAD51 foci formation in WT, *BRCA1$^{\Delta 11}$* and *BRCA1$^{\Delta 11}$53BP1^{S25A}* B cells 4 hours after 10 Gy IR, relative to WT. Statistical significance was determined by Mann-Whitney t-test.

Figure S4. Related to Figure 4

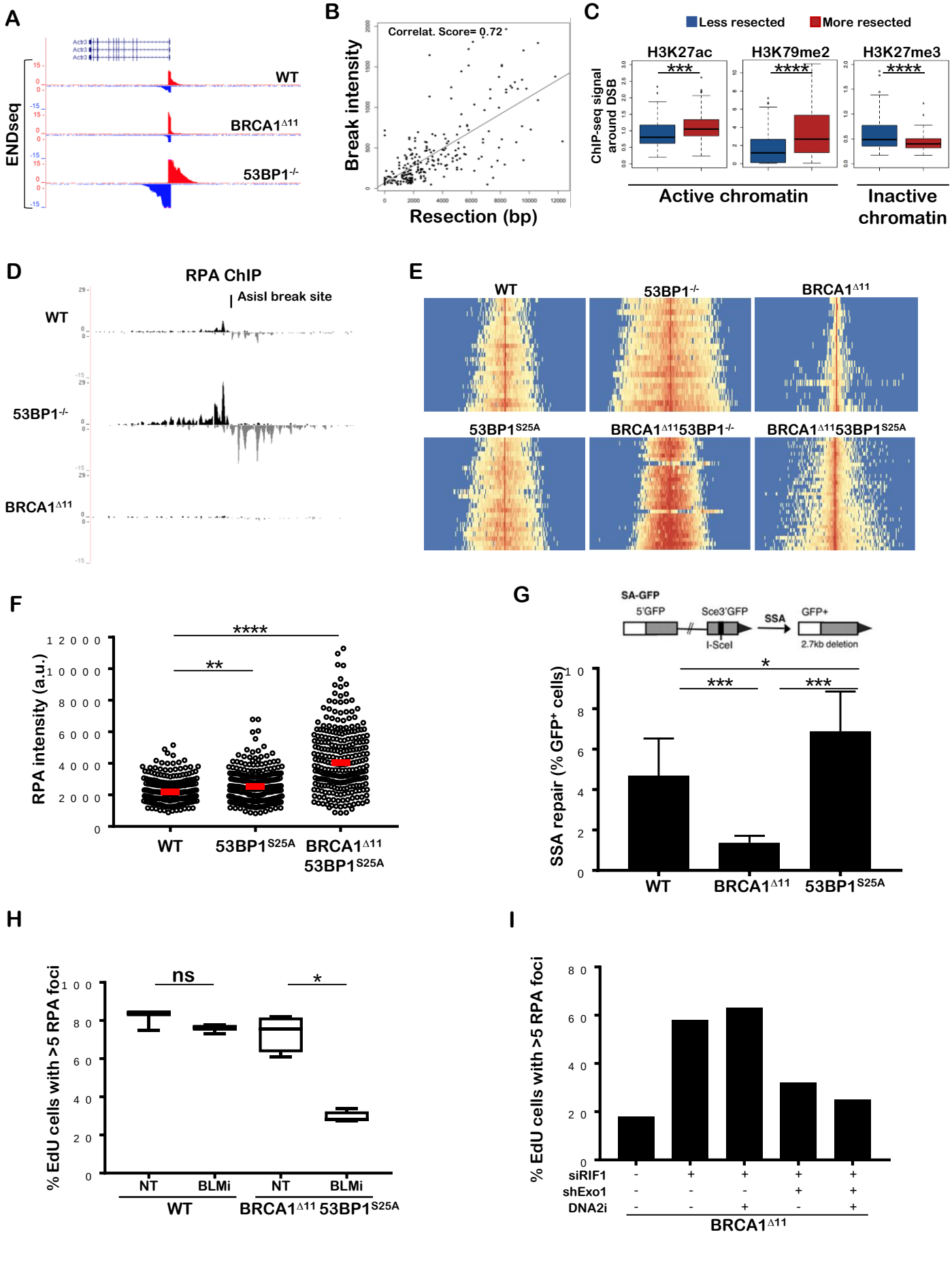

Fig. S4

Re-wiring of end resection in *BRCA1^{D11}53BP1^{S25A}* cells

(A) Genome browser snapshots showing END-seq signal at an individual AsiSI site 5 hours after AsiSI induction, demonstrating decreased resection in *BRCA1^{D11}* cells and increased resection in *53BP1$^{-/-}$* relative to WT. (B) Variation in end resection in WT MEFs correlates with AsiSI break intensity across the genome. (C) Regions with increased resection signal tend to harbor active chromatin marks (H3K27ac and H3K79me2), whereas lowly resected regions tend to enrich for inactive marks (H3K27me3). ChIPseq data was retrieved from the public study GSE90893 (https://www.ncbi.nlm.nih.gov/geo/query/acc.cgi?acc=GSE90893). Statistical significance was determined by Welch's t-test. (D) Genome browser snapshots showing representative examples of ChIP-seq for ssDNA-bound RPA at an AsiSI break site 5 hours after AsiSI induction. MEFs from the indicated genotypes were used. (E) Heat map of top 10% END-seq signals across individual AsiSI sites in WT, *53BP1$^{-/-}$*, *BRCA1^{D11}*, *53BP1S25A^{S25A}*, *BRCA1^{D11}53BP1$^{-/-}$* and *BRCA1^{D11}53BP1S25A^{S25A}* MEFs measured 5 hours after AsiSI induction. (F) Quantification of the intensity of chromatin bound RPA in individual EdU^{+} nuclei from WT, *53BP1^{S25A}* and *BRCA1^{D11}53BP1^{S25A}* MEFs. Cells were treated with 10 Gy and analyzed 4 hours post-IR. Statistical significance was determined by the Mann-Whitney t-test. (G) Top: Diagram of the SSA reporter substrate SA-GFP. Bottom: Relative frequency of SSA in WT, *BRCA1^{D11}* and *53BP1^{S25A}* MEFs. Cells stably transfected with SA-GFP were co-transfected with an I-SceI expression vector or control GFP expression vector. The GFP values from the I-SceI transfections were divided by the value from the control GFP transfection to normalize for transfection efficiency. Plots represent data from 9 independent transfected wells. Mann-Whitney t-test was used to determine statistical significance. (H) Quantification of RPA foci formation in EdU^{+} nuclei from WT and *BRCA1^{D11}53BP1^{S25A}* MEFs 4 hours after 10 Gy IR either pre-treated or not with 50 mM BLMi as described (Nguyen et al., 2013). Statistical significance was determined by the Mann-Whitney t-test. (I) Quantification of RPA foci formation in EdU^{+} nuclei from *BRCA1^{D11}* MEFs and their derivatives that are deficient in EXO1 and/or RIF1, either pre-treated or not with 1 mM DNA2i prior to 10 Gy IR. Cells were analyzed 4 hours post-IR.

Figure S5. Related to Figure 5

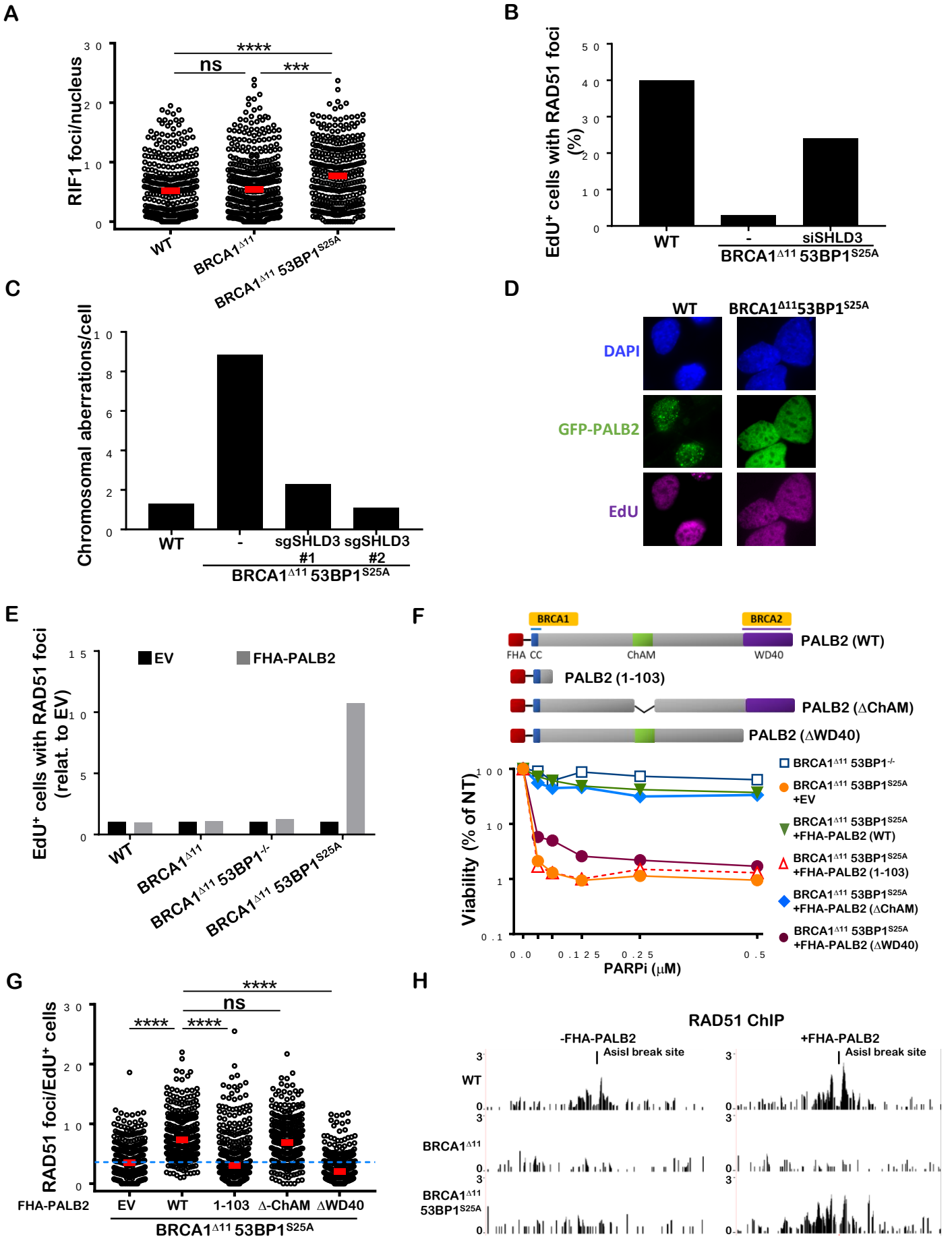

Fig. S5.

Shieldin-enforced block on PALB2/RAD51 loading and HR post-resection can be overcome by forced targeting of PALB2/BRCA2 to damaged chromatin

(A) Quantification of RIF1 foci in individual nuclei from WT, *BRCA1*$^{\Delta 11}$ and *BRCA1*$^{\Delta 11}$*53BP1*^{S25A} MEFs 1 hour after 10 Gy IR. Significance was determined by the Mann-Whitney t-test. (B) Quantification of EdU^{+} nuclei with RAD51 foci in *BRCA1*$^{\Delta 11}$*53BP1*^{S25A} MEFs and *BRCA1*$^{\Delta 11}$*53BP1*^{S25A} MEFs expressing SHLD3 siRNA. Cells were analyzed 4 hours after IR. (C) Quantification of chromosomal aberrations in *BRCA1*$^{\Delta 11}$*53BP1*^{S25A} MEFs and two independent derivative clones where SHLD3 was deleted by CRISPR-Cas9. Cells were treated with PARPi and metaphase spreads were assayed 16 hours later. (D) Representative images of GFP-PALB2 foci formation in WT and *BRCA1*$^{\Delta 11}$*53BP1*^{S25A} MEFs stably expressing GFP-PALB2. Cells were stained with GFP (green), counterstained with DAPI (blue) and EdU was detected using the Click-IT EdU kit (purple). (E) Fold changes in RAD51 IRIF formation in EdU^{+} cells of the indicated genotypes expressing either FHA-PALB2 or an empty vector (EV). Complementation with FHA-PALB2 increases RAD51 IRIF approximately 10-fold in *BRCA1*$^{\Delta 11}$*53BP1*^{S25A} MEFs but does not alter RAD51 foci formation in WT, *BRCA1*$^{\Delta 11}$ or *BRCA1*$^{\Delta 11}$*53BP1*$^{-/-}$ MEFs. (F) Top: Schematic representation of WT and mutant FHA-PALB2 constructs. Bottom: Viability of *BRCA1*$^{\Delta 11}$*53BP1*^{S25A} MEFs and derivatives that express different FHA-PALB2 constructs (depicted above), as measured by CellTiter-Glo 10 days after PARPi treatment. Viability of *BRCA1*$^{\Delta 11}$*53BP1*$^{-/-}$ MEFs was shown for comparison. (G) RAD51 foci per EdU^{+} nucleus in *BRCA1*$^{\Delta 11}$*53BP1*^{S25A} MEFs expressing the indicated forms of FHA-PALB2 measured 4 hours after 5 Gy IR. Foci numbers are normalized by nuclear area (per 100 μm^2). Significance was determined by the Mann-Whitney t-test. (H) Representative example of RAD51 ChIP-seq reads at an AsiSI break 5 hours after AsiSI induction in WT, *BRCA1*$^{\Delta 11}$ and *BRCA1*$^{\Delta 11}$*53BP1*^{S25A} MEFs with or without FHA-PALB2 complementation.

Figure S6. Related to Figure 1-6

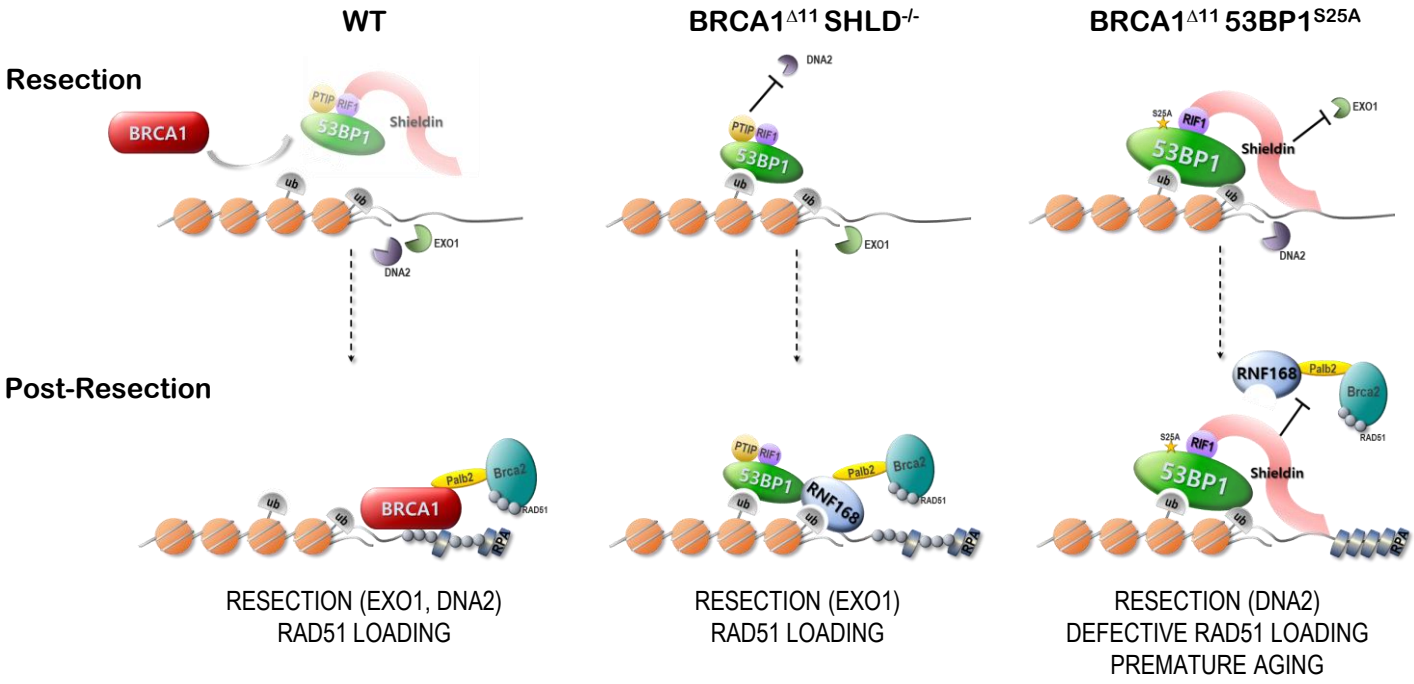

Fig. S6.

Proposed model for how PTIP and RIF1/Shieldin regulates HR.

In WT cells (left), BRCA1 inhibits 53BP1 interaction with chromatin proximal to DNA ends. This permits EXO1 and DNA2 nucleases to process the ends. BRCA1 subsequently facilitates the loading of RAD51 post-resection by recruiting PALB2/BRCA2 to ssDNA. In *BRCA1$^{\Delta 11}$SHLD$^{-/-}$* cells (middle), PTIP blocks DNA2 but DSBs become permissive for EXO1-mediated resection. In the absence of functional BRCA1 and without interference from Shieldin post-resection, RNF168 recruits PALB2/BRCA2 to load RAD51 onto ssDNA, thereby rescuing HR. In *BRCA1$^{\Delta 11}$53BP1^{S25A}* cells (right), RIF1/Shieldin blocks EXO1-mediated resection while DNA2-mediated end processing becomes permissive. However, the continued presence of Shieldin on ssDNA post-resection inhibits the accumulation of RNF168, which disables the recruitment of PALB2/BRCA2, impairing the loading of RAD51.